

Gravity of the Arctic Ocean from satellite data with validations using airborne gravimetry: Oceanographic implications

David C. McAdoo,² Sinead Louise Farrell,^{1,2,4} Seymour Laxon,^{3,5} Andy Ridout,³ H. J. Zwally,⁴ and Donghui Yi⁴

Received 27 September 2012; revised 19 December 2012; accepted 7 January 2013; published 25 February 2013.

[1] Precise mappings of sea surface topography, slope, and gravity of the Arctic Ocean are derived from altimeter data collected by Envisat and ICESat. Both altimeters measured instantaneous sea surface height at leads in the sea ice. To reduce contamination by ice-freeboard signal and tracker noise in Envisat height data, a retracking of the waveform data was performed. Analogous reprocessing of ICESat data was also done. Arctic mean sea surfaces (MSSs) were computed from Envisat data spanning 2002–2008 and ICESat data spanning 2003–2009. Farrell et al. (2012) used these “ICEn” MSSs to estimate mean dynamic topography (MDT). These same Envisat and ICESat data are used, in sea-surface-slope form, to compute the ARCTic Satellite-only (ARCS-2) altimetric marine gravity field. ARCS-2 extends north to 86°N and uses GRACE/GOCE gravity data (GOCO02S) for its long-wavelength (>260 km) components. Use of Envisat data improves the spatial resolution over that of existing Arctic marine gravity fields in many areas. ARCS-2’s spatial resolution aids in tracing tectonic fabric—e.g., extinct plate boundaries—over broad areas of the Arctic basin whose tectonic origin remains a mystery. ARCS-2’s precision is validated using NASA 2010/2011 Operation IceBridge (OIB) airborne gravimetry. ARCS-2 and OIB gravity along with ICEn-MSS results are employed to locate short-wavelength errors approaching 1 m in current Arctic marine geoids (EGM2008). Precise OIB airborne gravity corroborates that such errors in current geoid/gravity models are widespread in Arctic areas lacking accurate surface gravity data. These geoid errors limit the spatial resolution at which MDT can be mapped.

Citation: McAdoo, D. C., S. L. Farrell, S. Laxon, A. Ridout, H. J. Zwally, and D. Yi (2013), Gravity of the Arctic Ocean from satellite data with validations using airborne gravimetry: Oceanographic implications, *J. Geophys. Res. Oceans*, 118, 917–930, doi:10.1002/jgrc.20080.

1. Introduction

[2] Of all the world’s ocean basins, the Arctic Ocean continues to be the most poorly understood basin insofar as its origin and tectonic history. Its remote location and persistent ice cover have limited access by surface research vessels [Laxon and McAdoo, 1994]. Moreover, the thick layers of sediments which fill most of the Arctic Ocean basin mask tectonic fabric imprinted in the sea floor making it

difficult to trace fossil and active mid-ocean ridge systems. Laxon and McAdoo [1994] demonstrated the potential of using altimetric gravity to help trace the tectonic fabric in the Arctic basin. The Arctic’s tectonic uncertainties are concentrated in that large portion of the Arctic Basin known as the Amerasian Basin (AB) [Grantz et al., 1990; Grantz et al., 2011; McAdoo et al., 2008] which encompasses both the Canada and Makarov Basins and comprised all the oceanic crust lying between the Lomonosov Ridge and North American/northeastern-most Asian margin. Absent a definitive tracing of a mid-ocean ridge system within the AB, the age and source of crust therein remain uncharted. Section 2 below includes a brief description of the Amerasian Basin and the obstacle it presents to understanding Arctic tectonics.

[3] Sandwell and Smith [2009] posit, quite justifiably, that “marine gravity anomalies derived from radar altimeter measurements of ocean surface slope are the primary data for investigating global tectonics and continental margin structure” and that these altimeter data “. . . are enormously valuable for exploring the remote ocean basins.” They also point out that “eight high-precision radar altimeter missions” beginning with Geosat in 1985 have made a very large amount of sea surface height measurements. However of these

All Supporting Information may be found in the online version of this article.

¹NOAA Laboratory for Satellite Altimetry, College Park, Maryland, USA.

²Earth System Science Interdisciplinary Center, Uni. Maryland, College Park, Maryland, USA.

³National Centre for Earth Observation-Centre for Polar Observation and Modelling, University College London, London, UK.

⁴Cryospheric Sciences Branch, NASA Goddard SFC, Greenbelt, Maryland, USA.

⁵Deceased 2 January 2013.

Corresponding author: D. C. McAdoo, NOAA Laboratory for Satellite Altimetry, College Park, MD, USA. (Dave.McAdoo@noaa.gov)

© 2013 American Geophysical Union. All Rights Reserved.
2169-9275/13/10.1002/jgrc.20080

eight radar altimeter missions only three—the European Space Agency’s (ESA’s) ERS-1, ERS-2, and Envisat—extend far enough north to cover much of the Arctic Ocean; all three ESA missions measure topography to 81.5°N . ESA’s new radar altimeter satellite [Wingham *et al.*, 2006] is now extending coverage of the Arctic Ocean topography north to 88°N .

[4] In this paper, we have extended Arctic altimetric gravity north to 86°N by incorporating high-resolution satellite laser altimetry data from the Geoscience Laser Altimeter System (GLAS) onboard NASA’s ICESat. Thus we have filled in 88%, by area, of the polar hole left by radar altimetry; the new Arctic Satellite-only (ARCS-2) altimetric gravity field (Figure 1) presented here is derived from a combination of an Envisat radar altimeter data set spanning 6 years (2002–2008) and an ICESat laser altimeter data set incorporating sixteen campaigns spanning the satellite’s operational lifetime, 2003–2009. ICESat’s GLAS data collection campaigns came to an end in 2009 and the satellite was decommissioned in 2010. Consequently we now have the GLAS data set for the total ICESat mission at hand. *McAdoo et al.* [2008] previously used a subset of early-release GLAS data together with ERS-2 radar altimetry to derive the Arctic Satellite-only (ARCS) altimetric gravity field—a forerunner to the

ARCS-2 gravity field presented here. However this earlier ARCS field used data from only five ICESat campaigns, representing about 30% of the GLAS data used here for computing the new ARCS-2 field. In addition, the GLAS data used in the computation of the ARCS field were an earlier version (GLAS data releases 18–26) than the 16 campaigns of data used herein (cf. section 3.1).

[5] In addition to the ICESat laser altimeter data, we also have used dual-frequency radar altimetry (RA-2) data acquired by ESA’s Envisat, over a 6 year time span (2002–2008) to compute this ARCS-2 marine gravity field. We used Envisat data in place of the ERS-2 data that were employed in the previous ARCS-1 field [McAdoo *et al.*, 2008]. The surface coverage of Envisat RA-2 while in its 35 day repeat orbit is virtually identical to that of ERS-2 in its 35 day repeat. But improved processing techniques including waveform reprocessing (or retracking) of selected summer/fall Envisat waveforms as described in section 3.2 dramatically reduces tracker “noise” due to sea ice and gives rise to better spatial resolution of sea surface topography (and hence marine gravity) than was achieved heretofore (e.g., with the ERS-2 data used before in the ARCS-1 field). These Envisat radar altimetry data are the main source of all the detailed marine gravity information in the new ARCS-2 field for all latitudes $<80^{\circ}\text{N}$.

[6] Techniques used in this paper to compute gravity anomalies from these altimeter data—both ICESat and Envisat—are updated versions of those used in *McAdoo et al.* [2008] and are outlined in section 3.3. These techniques are similar in concept to those used by *Haxby et al.* [1983], *Sandwell and Smith* [1997], and *Sandwell and Smith* [2009] and begin with the measurement of ocean surface slopes along the ground tracks of each ICESat and Envisat altimeter pass. In the absence of the wind, tides, and ocean dynamics, these ocean surface slopes are identical to geoid slopes (or deflections of the vertical). These ICESat and Envisat slopes are then used to compute the short-wavelength (<450 km) component of the marine gravity field. We show that the resulting ARCS-2 marine gravity field has much better spatial resolution than the first such radar altimetric marine gravity field of the Arctic derived by *Laxon and McAdoo* [1994], from a single 35 day cycle of retracked ERS-1 data. We also show that this ARCS-2 field compares favorably with—and often surpasses—the resolution of other altimetric gravity fields specifically: (a) the Arctic ARCS-1 field [McAdoo *et al.*, 2008] which it does surpass in resolution and (b) the global field of *Sandwell and Smith* [2009] whose resolution in the Arctic appears to be no better than that of ARCS-2. Comparisons are also shown with gravity fields of the Arctic, e.g., the Earth Geopotential Model or EGM2008 [Pavlis *et al.*, 2008] and ArcGP [Kenyon and Forsberg, 2008] which are predominantly—but not exclusively—gravimetric inasmuch as some satellite altimeter data are used where necessary to fill areas which lack direct surface observations of gravity. Note that for all the Arctic Ocean north of 60°N EGM2008 is derived from ArcGP and so includes the short-wavelength errors that exist in ArcGP. Globally, the EGM2008 geopotential model is derived from surface—or near-surface—gravimetry, as well as GRACE data and tends to yield an accurate geoid of the global oceans with RMS error of about 6 cm [Pavlis *et al.*, 2008]. However of all the world’s oceans, the Arctic presents a unique

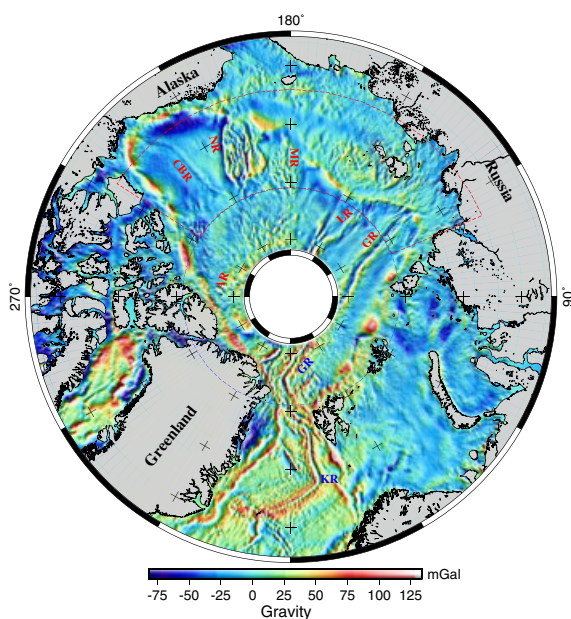


Figure 1. Arctic Satellite-only (ARCS-2) marine gravity field computed using a combination of 16 campaigns of reprocessed ICESat/GLAS sea surface elevations and retracked Envisat altimeter waveform data spanning seven summers (2002–2008). Latitude-longitude box F2 outlined in red dashes delineates the area covered in Figure 2. Blue dashes lie along the 80.5°N parallel, south of which ARCS2 gravity is computed entirely from Envisat data and north of which ARCS2 is computed almost entirely from ICESat data. Note that labeled in red are the gravitational expressions of the Gakkel Ridge (GR), the Lomonosov Ridge (LR), the Mendeleev Ridge (MR), the Northwind Ridge (NR), the Alpha Ridge, and the buried, extinct Canada Basin Ridge (CBR) and labeled in blue are the Knipovich Ridge (KR) at the northern end of the Mid-Atlantic Ridge and the western portion of the Gakkel Ridge (GR). See text.

challenge to marine geoid mapping owing to (a) sea ice which historically has made surface gravimetry (e.g., from surface ships) difficult and (b) the subtle Arctic MDT signal which places particularly stringent requirements on geoid accuracy. In contrast to ArcGP (and EGM2008), the ARCS-2 field is a satellite-only field. ARCS-2 uses no surface gravity data and is thus free of errors associated with direct observations of surface gravity and affords an independent comparison for models based on surface gravity.

[7] Because the long-wavelength (>400 km) gravity field is more accurately measured from orbit by satellites such as GOCE [Pail *et al.*, 2010; Rummel *et al.*, 2011] and GRACE [Tapley *et al.*, 2004] than by any other means, we employ gravity from the new GRACE/GOCE satellite-only models, GOCO01S [Pail *et al.*, 2010] and GOCO02S [Goiginger *et al.*, 2011] in a remove-restore procedure to provide this long-wavelength component of the ARCS-2 field.

[8] We then compare our new ARCS-2 field with the existing EGM2008 gravity field primarily to identify localized, short-wavelength errors in the ArcGP field. (We will show that these errors in the ArcGP field tend to occur at the gaps in the coverage of the input surface, submarine, and airborne data used in ArcGP.) Also, to quantitatively assess and validate the ARCS-2 gravity field, we use in section 4 airborne gravity measurements collected over the Arctic in 2010 and 2011 by NASA as part of its Operation IceBridge (OIB) campaign [Cochran *et al.*, 2011; Cochran and Bell, 2010]. By comparing these state-of-the-art OIB gravity data with results from the ARCS-2 and ArcGP gravity fields, we can attribute discrepancies between ArcGP and OIB gravity in specific areas of the Arctic Ocean to short-wavelength errors in the ArcGP gravity field and, hence, geoid. In fact our first means of isolating and detecting errors in existing geoid models such as ArcGP (or EGM2008) is direct comparison of gravity anomalies predicted by these models with the new (2010 and 2011), high accuracy OIB airborne gravity. Without this OIB gravity, we cannot unambiguously attribute ArcGP-ARCS2 differences to errors specifically in either ArcGP or ARCS-2. Wherever a large gravity anomaly error is detected in the EGM 2008 model, a corresponding geoid error exists in the EGM 2008 geoid model. Actual geoid errors can then be estimated with Stokes integral transform.

[9] These relatively large errors in the ArcGP (and EGM2008) geoid pose a major obstacle for oceanographers trying to determine the mean dynamic topography (MDT)—and hence geostrophic circulation—of the Arctic Ocean. Wunsch and Gaposchkin [1980] pointed out that mean sea surface, or MSS, heights derived from satellite altimetry could be combined with a precise geoid to derive the mean dynamic topography (MDT). Indeed Tapley *et al.* [2003] showed that a geoid derived solely from GRACE satellite data can be differenced from a mean sea surface derived from TOPEX/POSEIDON, ERS-1, -2 and Geosat altimetry to derive the MDT and large-scale circulation of the non-polar global ocean. However, in the Arctic Ocean, Farrell *et al.* [2012] show that geoid errors present a greater challenge to determining an accurate, detailed MDT. MSSs such as the ICEn (or ICESat-Envisat) MSS [Farrell *et al.*, 2012], while conforming closely to the geoid, are actually the superposition of the relatively large geoid height signal with the relatively small signal of the mean dynamic ocean topography, or MDT. In fact, we identify, in section 5 below,

some short-wavelength errors in current Arctic marine geoid models by comparing and differencing the ICEn MSS model with the EGM2008 geoid model. This comparison of the ICEn MSS with the EGM2008 geoid provides a second means (comparisons described above with the new OIB gravity data being the first means) to identify some remaining short-wavelength errors in current Arctic marine geoid models. Our companion paper, Farrell *et al.* [2012] has indicated that short-wavelength geoid errors limit our current ability to map details of the Arctic MDT. So, in this paper we identify and characterize—as a function of wavelength—geoid errors in the state-of-the-art Arctic models. We thereby estimate and quantify the improvements which are needed in detailed Arctic geoids before detailed, small-scale structures of Arctic Ocean circulation such as stationary eddies can be confidently resolved. Realization of an accurate MDT for the Arctic Ocean requires an accurate new Arctic geoid—more accurate than current geoids—and completion of such a geoid will require an abundance of new Arctic gravity observations particularly in areas now lacking in such observations.

2. Tectonics of the Arctic Ocean Basin: A Brief Background

[10] Laxon and McAdoo [1994], Forsberg and Skourup [2005], and McAdoo *et al.* [2008] have demonstrated the potential of using altimetric gravity to help trace the tectonic fabric in the Arctic basin. Because the focus of this paper—in contrast to McAdoo *et al.* [2008]—is more on the oceanographic than geotectonic applications of satellite altimetry, Arctic tectonics are only briefly reviewed here. Among the world's major ocean basins the Arctic basin stands out as having the most uncertain tectonic history. The Arctic Basin comprised two parts: the relatively young, Eurasian Basin, which has formed in the past 55 Ma and lies on the Atlantic side of the Lomonosov Ridge (LR; see Figure 3) and the older, larger Amerasian Basin (AB) which lies on the Pacific side of the LR. The Eurasian Basin (EB) has formed via sea floor spreading along the Gakkel Ridge [Brozena *et al.*, 2003; Cochran *et al.*, 2003] which remains active at present time; the EB's tectonic history is rather well understood. On the other hand, the AB has an uncertain, controversial, and complex tectonic history. An extensive literature [e.g., Grantz *et al.*, 1990; Grantz *et al.*, 2011; McAdoo *et al.*, 2008] describes the tectonic enigma of the AB. Tectonic models of AB's formation differ widely but generally concur that the AB formed in the late Mesozoic and is tectonically inactive at present. Controversies about the AB include how its Canada Basin portion (see Figure 3) formed. Grantz *et al.* [2011] along with Laxon and McAdoo [1994] [cf. Cochran *et al.*, 2006; Taylor *et al.*, 1981] suggested the Canada Basin opened via seafloor spreading along a now-extinct Canada Basin Ridge (CBR, see Figure 1).

3.1. ICESat/GLAS Data

[11] The Geoscience Laser Altimeter System (GLAS) onboard ICESat provides high-resolution satellite laser altimetry data (~ 70 m footprints spaced at 172 m along track) with coverage of the Arctic to 86°N [Zwally *et al.*, 2002] and a range precision of ~ 2 cm over flat sea ice surfaces [Kwok *et al.*, 2004]. The mission was conducted in campaign mode,

where each laser campaign lasted approximately 33 days, with between 2 and 3 campaigns per year [Yi *et al.*, 2011]. We use ICESat data collected between October 2003 (Laser 2a) and April 2009 (Laser 2e). Specific laser operation dates are described at http://nsidc.org/data/icesat/laser_op_periods.html. The data used are Release 428 and have been processed using precision orbit, tidal, and saturation corrections. The isostatic inverse barometer correction has been applied and cloud-filtering techniques are used to exclude data corrupted by forward scattering [see Zwally *et al.*, 2008; Yi *et al.*, 2011 for further details].

[12] Along-track instantaneous sea surface height (SSH) was calculated for the ice-covered Arctic Ocean following the methodology described by Zwally *et al.* [2008], which is based on the assumption that the small diameter of the GLAS footprint discriminates thin ice and narrow leads [Kwok *et al.*, 2004]. The local SSH is calculated for each GLAS footprint by taking the mean of the lowest 2% of the elevation distribution of data within ± 25 km of the local footprint. Selected empirically, the 2% value provides enough data to reduce measurement noise, however in the event that no leads exist within the 50 km search range, the SSH will be overestimated. Farrell *et al.* [2009] have shown that leads observable by ICESat are densely distributed across the Arctic Ocean; notable exceptions are parts of the Canadian Arctic Archipelago, the northwestern coast of Ellesmere Island, and the northern coastline of Greenland where an absence of leads in thick, consolidated multiyear ice or fast ice prevents SSH estimation. SSH is estimated at 40 Hz along-track resolution (i.e., an estimate is made for every reference footprint) along each ICESat orbit. An along-track MSS is computed for each orbit, by stacking and averaging repeat passes gathered during the observation period. Farrell *et al.* [2012] show that the ~ 170 m along-track sampling provided by ICESat resolves steep sea surface slopes particularly nearby continental shelf breaks and over narrow bathymetric features.

[13] The northern portion (latitudes $> 81.2^\circ\text{N}$) of our ARCS-2 altimetric marine gravity field (Figure 1) is computed using exclusively 16 campaigns of reprocessed ICESat/GLAS sea surface elevations. For an ICESat/GLAS-only marine gravity field extending south to 76.0°N (see Figure S1). Between 80.5°N and 81.2°N , ARCS-2 gravity is a blend of ICESat and Envisat altimetric gravity. This blending is done using a weighted mean where weights vary linearly with latitude such that at 81.2°N ICESat gravity receives full weight and Envisat gravity zero weight, whereas at 80.5°N the ICESat-Envisat weighting is reversed. Note that south of 80.5°N , ARCS-2 gravity is computed solely from Envisat data (see section 3.2 just below).

3.2. Envisat Radar Altimeter Data

[14] The European Space Agency's (ESA's) Envisat profiles sea surface topography using a dual-frequency, Ku- and S-band, pulse-limited Radar Altimeter-2 (RA-2). The returned radar power echoes, or waveforms, are used to correct RA-2 range errors thereby reducing or nearly eliminating tracker noise [cf. Giles *et al.*, 2007, 2008]. A single, best 35 day repeat cycle is chosen from each late-summer (August/September) season from 2002 to 2008 and reprocessed or "retracked." The selection of late summer data is intended to recover a predominance of specular echoes or waveforms

best suited for isolating lead or ocean elevations. The retracking process includes sub-selection of only the specular RA-2 waveforms to extract precise sea surface heights over leads (as opposed to diffuse waveforms which yield ice floe heights) within the ice-covered Arctic Ocean and is essentially the processing described by Giles *et al.* [2008], Peacock and Laxon [2004], and Laxon [1994]. These seven 35 day cycles of retracked RA-2 sea surface elevations are then stacked, or averaged. Applied orbit and tide corrections are described by Farrell *et al.* [2012] and inverted barometer corrections use the model of Carrere and Lyard [2003].

[15] The southern portion of our ARCS-2 altimetric marine gravity field is computed using reprocessed Envisat sea surface elevations from the 7 year time span 2002–2008 (see Figure S2). Our processing and use of Envisat data in ARCS-2 enables the recovery of finer gravity detail than was possible with the ERS-2 data used in the ARCS field [McAdoo *et al.*, 2008]. This finer gravity detail recovered by using the Envisat data in ARCS-2 is evident in Figure 2 particularly over the Chukchi Borderland area (longitudes from 194.0°E to 204.0°E), over the northern Laptev Sea (from 126.0°E to 140.0°E , and 76.5°N to 80.0°N) where the Nansen Gakkel ridge intersects the Eurasian continental shelf break, and over the Sverdrup Spur area (near 232°E , 80°N). Figure S3a in the supporting information also reveals this increased gravity detail recovered from Envisat data. This increased detail recovered by using Envisat data is confined to the southern portion of the ARCS-2 field (latitudes $< 80.4^\circ\text{N}$). The northern portion ($> 81.2^\circ\text{N}$) of the ARCS-2 field is computed exclusively from ICESat data and may not recover gravity details as fine as in the southern portion.

3.3. ARCS2 Altimetric Gravity Field Computation

[16] Techniques used here for computing ARCS2 gravity are updated versions of those used in McAdoo *et al.* [2008] for ARCS-1. But Envisat data (section 3.1 above) are now used in place of ERS-2 data. Again, our methods are conceptually similar to those used by Haxby *et al.* [1983], McAdoo and Marks [1992], Sandwell and Smith [1997] and Sandwell and Smith [2009]. After reprocessing both ICESat and Envisat

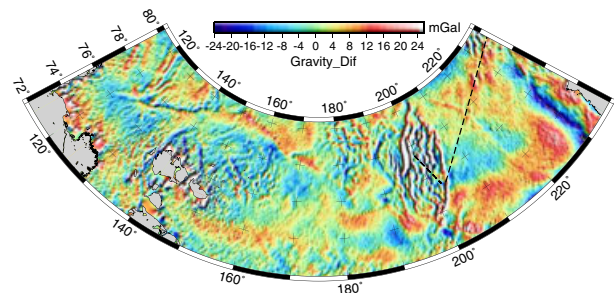


Figure 2. ARCS-2 gravity from Envisat minus ARCS gravity from ERS-2 [see McAdoo *et al.*, 2008] within the lat-lon box F2 shown in Figure 1. The details recovered by use of Envisat data in ARCS-2 versus the somewhat smoother ERS results in ARCS-1 are evident. Dashed black lines denote where airborne gravity data were collected on Operation IceBridge flight, “Sea Ice 1” 19 April 2010 (see Appendix A and Figures S3a and S3b). Short NW-SE trending flight line profiled in Figure S3a and long SW-NE trending line in Figure S3b.

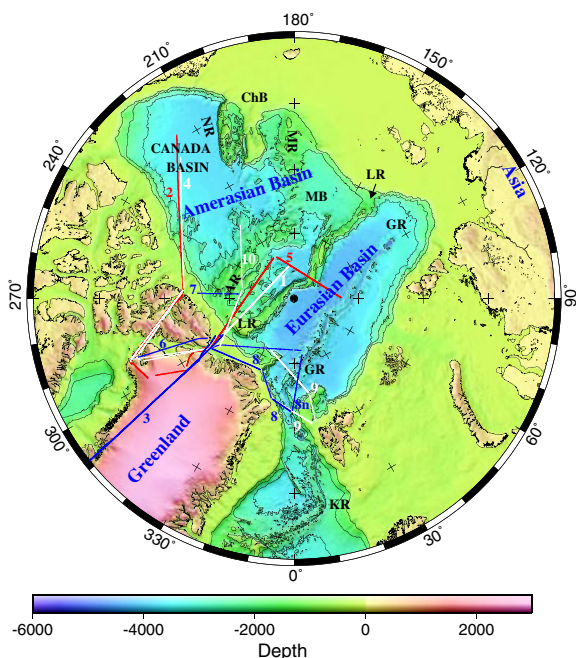


Figure 3. Bathymetry of the Arctic from IBCAO-v2 data grid [Jakobsson *et al.*, 2008]. Contours are drawn at 1000, 2000, and 3000 m depths. Note large-scale physiographic features particularly the Eurasian Basin and the Amerasian Basin, which are separated from each other by the Lomonosov Ridge (LR). Other labeled physiographic features include the Alpha Ridge (AR), the Mendeleev Ridge (MR), the Makarov Basin (MB), the Chukchi Borderlands (ChB), the Northwind Ridge (NR), the Gakkel Ridge (GR), an active, slow spreading ridge tracing down the middle of the Eurasian Basin, and the Knipovich Ridge (KR). Compare this bathymetry with gravity in Figure 1. Operation IceBridge (OIB) airborne gravity lines from nine different flight days during the OIB 2010 and 2011 campaigns. Line 1 (white) is profiled in Figure 4a below; Line 2 (red) is profiled in Figure 4b below. Line 3 (blue) is profiled in Figure 4c. Line 4 (white) is profiled in Figure 4d. Line 5 (red) is profiled in Figure 4e. Line 6 (blue) is profiled in Figure 4f. Line 7 (blue) is profiled in Figure 4g. Line 8 (blue) is profiled (north-south trending segment, 8n, over the GR) in Figure 4g. Line 9 (white) is coincident with line 8 where it traces along the Greenland shelf edge and this coincident portion is profiled in Figure S4. Line 10 (white) is profiled in Figure S5.

altimetry waveforms using satellite-specific techniques described in sections 3.1 and 3.2 above, we are left with along-track profiles of sea surface topography which are accurate indicators of gravity in the wavelength band 20–450 km. Along-track sea surface height profiles are then edited for outliers, band-pass filtered, and processed following McAdoo *et al.* [2008] to estimate, in two separate processes, along-track slopes for both ICESat and Envisat data.

[17] We construct two separate Arctic marine fields: (1) an ICESat-only gravity field using just the ICESat along-track, sea surface slopes (see section 3.1) and (2) an Envisat-only field using just the Envisat along-track slopes (see section 3.2) following same methods of McAdoo *et al.* [2008] using ICESat and ERS-2 slopes. To begin, we compute the four along-track slope grids (two each—ICESat and Envisat)

before the slopes are low-cut filtered, by gridding with continuous curvature splines [Wessel and Smith, 1998] and by filling in the void over land with pseudo-slopes computed by assuming that land gravity conforms exactly to the smoothed long-wavelength, GRACE/GOCE, GOCO02S satellite-only geopotential [Pail *et al.*, 2010; Goiginger *et al.*, 2011] described below. Because ARCS2 is to be a satellite-only field, no land gravimetry is used. Each of these four along-track slope grids is low-cut filtered by removing from these slopes a long-wavelength (>260 km) background geoid slope field, derived entirely from the GOCO02S geopotential model [Goiginger *et al.*, 2011]. Resulting band-limited along-track geoid slope fields are then converted via vector algebra into true deflections of the vertical (north and east components) (see equations (3a) and (3b) in McAdoo and Marks [1992], or Appendix B in Sandwell and Smith [1997]). Resulting deflection-of-vertical grids are Fourier transformed using conventional FFT techniques and then input to inverse Vening Meinesz transformation to obtain to short-wavelength, altimetric gravity anomalies (see McAdoo *et al.* [2008]; also equation (A8) of McAdoo and Marks [1992]). Note that the forward—as opposed to the inverse—Vening Meinesz transformation for computing deflections of the vertical from gravity anomalies is given in section 2-22 of Heiskanen and Moritz [1967] and originally in Vening Meinesz [1928]. The long-wavelength background GOCO02S gravity field [Goiginger *et al.*, 2011] is then added back or restored to the short-wavelength altimetric gravity to obtain (1) the final ICESat-only gravity field (section 3.1 and Figure S1) and separately (2) the final Envisat-only field (section 3.2 and Figure S2).

[18] The ICESat-only and Envisat-only gravity fields are then spliced together as described in Section 3.1 above to form the ARCS2 gravity field (Figure 1). The northern portion (latitudes $>81.2^\circ$ N) of the ARCS-2 gravity field is computed entirely from ICESat-only gravity and the southern portion (latitudes $<80.5^\circ$ N) from Envisat-only gravity. Between 80.5° N and 81.2° N ARCS-2 gravity is a blend of ICESat and Envisat altimetric gravity.

4. IceBridge Airborne Gravity for Validating Gravity Models and Detecting Errors

[19] State-of-the-art airborne gravity measurements have been collected over the ice-covered Arctic Ocean during March–April 2010, and 2011 by NASA as part of its airborne Operation IceBridge (OIB) mission [see <http://www.nasa.gov/icebridge/>]. OIB is a multi-year, multi-sensor NASA airborne mission [Koenig *et al.*, 2010] aimed at observing changes in the Arctic and Antarctic ice sheets, ice shelves and sea ice. The gravimeter is just one instrument in a suite of airborne sensors used on OIB flights. Over ice sheets and shelves, respectively, the OIB gravity data are used to estimate sub-ice bedrock topography and bathymetry. However, over the sea ice, OIB gravity may be used to improve determination of the geoid in areas such as the northern Arctic Ocean where gravity/geoid models are particularly lacking precise, detailed gravity data. Accurate, detailed geoid information is needed to precisely determine sea ice freeboard and sea surface anomalies along the OIB flight lines. OIB Arctic gravity data used here were collected with the NASA DC-8 in 2010 and the NASA P-3 in 2011 and are publically available as GRAV

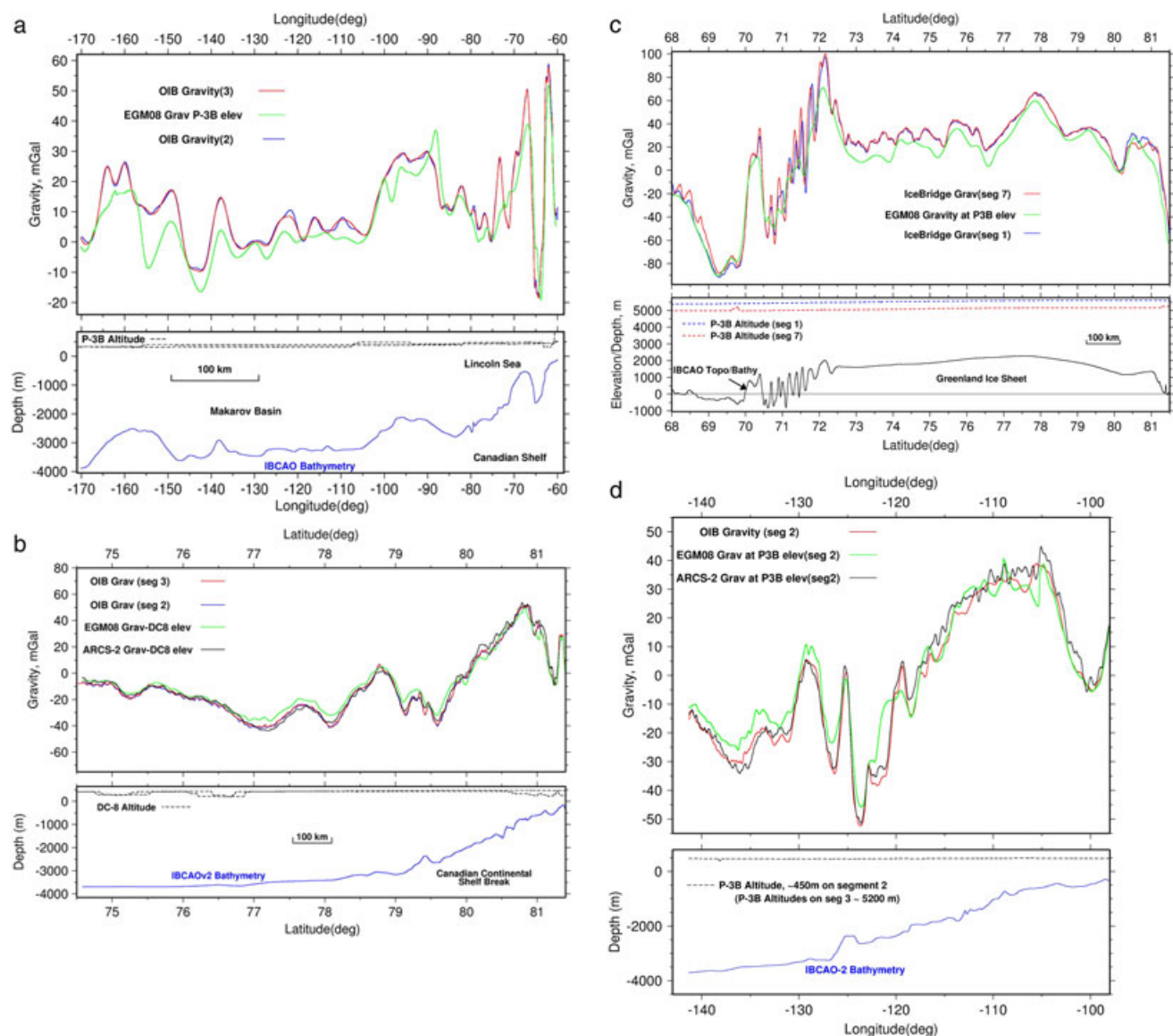


Figure 4. (a) OIB airborne gravity anomalies from 17 March 2011 P-3B underflight of CryoSat-2 (see line 1 in Figure 3). Near-repeat out and back legs (blue and red respectively) were both flown at low elevation (order 400 m). EGM2008 gravity prediction along flight path at P-3B aircraft elevation is shown in green. (b) OIB airborne gravity anomalies from 5 April 2010 DC-8 underflight of Envisat (see line 2 in Figure 3). Near-repeat out and back legs (blue and red, respectively) are both flown at low elevation. EGM2008 gravity prediction along flight path at DC-8 aircraft elevation is shown in green. (c) OIB airborne gravity anomalies from 15 April 2011 CryoVex line (southern portion overlying Greenland), see line #3 in Figure 3. Near-repeat out (segment 1) and back (segment 7) legs (blue and red, respectively) are flown at elevations of about 5380 and 5100 m, respectively. EGM2008 gravity prediction along flight path at P-3B aircraft elevation is shown in green. (d) OIB airborne gravity anomalies from the 16 March 2011 underflight of Envisat (see line #4 in Figure 3) are plotted in red. Note that this ground track differs slightly from Envisat track, line 2, flown on 5 April 2010 (see Figures 3 and 4b). The outbound (segment 2) and return (segment 3) portions are flown at quite different elevations of about 450 and 5200 m, respectively. Only the OIB gravity for the low-elevation, outbound segment #2 is shown here. (e) OIB airborne gravity anomalies (dashed red and solid blue) from the 20 April 2010 underflight of CryoSat-2. See line 5 in Figure 3. The outbound (segment 6) and return (segment 7) portions are flown at quite different elevations of about 6850 and 440 m, respectively. Only EGM2008 gravity prediction at the low elevations (~ 400 m) are plotted (in green) to compare with the low-elevation OIB gravity (in blue) for segment 7. (f) OIB airborne gravity anomalies (blue) from 18 March 2011 “ZigZag West” flight outbound segment (see line #6 on Figure 3) up the Nares Strait versus EGM2008 gravity prediction (green) at P-3B aircraft elevation (2000–5100 m). (g) OIB airborne gravity anomalies (blue) from 18 March 2011 “ZigZag West” flight segments 4 and 5 north of Ellesmere Island versus EGM2008 gravity prediction (green). See line # 7 on Figure 3. ARCS-2 gravity prediction is shown in red. (h) OIB airborne gravity anomalies (blue) from 28 March 2011 “Fram Strait Gateway” versus EGM2008 gravity prediction (green). See line #8n on Figure 3.

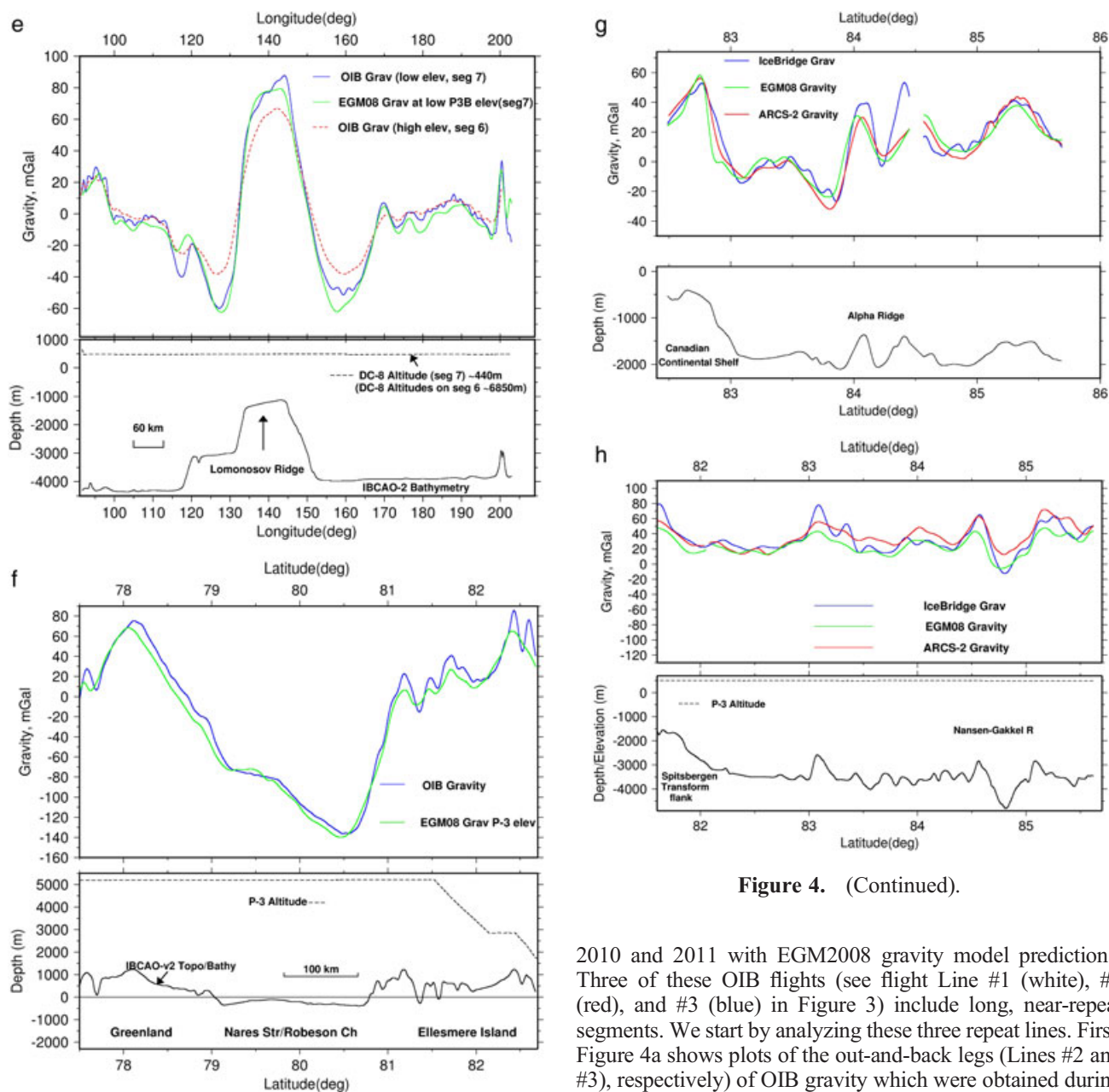


Figure 4. (Continued).

Figure 4. (Continued).

L1B Geolocated Free-Air Anomalies (IGGRV1B; see http://nsidc.org/data/icebridge/data_summaries.html#airgrav). OIB gravity data were obtained using a Sander Geophysics Ltd (SGL) Airborne Inertially Referenced Gravimeter (AIRGrav) and were processed by SGL and Lamont Doherty Earth Observatory personnel as described in Cochran *et al.* [2011] and Cochran and Bell [2010]. Studinger *et al.* [2008] presented flight validations of the AIRGrav system prior to OIB flights.

[20] Since the OIB sea ice lines are typically flown in long (of order 1000 km), straight, nearly constant, and low-altitude (400–500 m) segments, they tend to produce very low inertial accelerations and provide particularly accurate gravity results. We analyze and compare (Figures 4a–4h) gravity obtained on seven OIB flight days in March/April

2010 and 2011 with EGM2008 gravity model predictions. Three of these OIB flights (see flight Line #1 (white), #2 (red), and #3 (blue) in Figure 3) include long, near-repeat segments. We start by analyzing these three repeat lines. First, Figure 4a shows plots of the out-and-back legs (Lines #2 and #3), respectively) of OIB gravity which were obtained during the low-altitude (350–450 m) under-flight of CryoSat-2 on 17 March 2011. The IceBridge gravity profiles 2 and 3 repeat closely. Repeatability or noise level (calculated from standard deviation of differences between #2 and #3) ranges from 0.36 to 0.85 mGal depending on choice of low-pass filtering adopted (nominal, 100 s filtering yields repeatability of 0.62 mGal, see Table 1). Corresponding differences between the OIB airborne gravity and the upward continued EGM2008 gravity (in green, Figure 4a) are much larger. In a number of places (see Figure 4a) these differences are about 20 mGal. The standard deviation of these EGM-OIB differences range from 4 to 8 mGal (for three different low-pass filter schemes). The standard deviation, 5.65 mGal, for EGM-OIB differences listed in Table 1, line #1, is for 100 s OIB-AirGRAV low-pass filtering.

[21] The second set of repeat lines (Figure 4b) of OIB gravity data was collected during the low-altitude (400–500 m) underflight of Envisat on April 5, 2010 and also repeat very closely [see also Cochran *et al.*, 2011;

Ferguson et al., 2010]. Noise levels (calculated from standard deviation of repeat differences) range from 0.3 to 0.7 mGal depending on choice of low-pass filtering (0.43 mGal standard deviation with nominal filter of 100 s, see Table 1).

[22] The third set of near-repeat lines (Figure 4c) of OIB gravity data was collected during the higher altitude CryoVex transits over west Greenland on 15 April 2011. A repeatability of 1.22 mGal (see Table 1) is calculated using the nominal filtering of 100 s which is good owing to the somewhat different flight elevation of ~5380 m (out/segment 1; see Figure 4c) and ~5100 m (back/segment 7).

[23] For all three repeat flights, i.e., lines #1–#3, the repeatabilities of 0.43–1.22 mGal listed in column 2 of Table 1 are high which attests to the precision of the OIB gravity data. In addition, two more OIB flights are repeated year over year—2010 DC-8 versus 2011 P-3B OIB gravity—with comparably good repeatabilities (see Appendix A, Figures S4 and S5). Indeed the repeatabilities in Table 1 are much smaller than the differences between OIB and EGM2008 gravity (see columns 3 and 4 of Table 1) owing for the most part to errors in the EGM2008 (or ArcGP) model in the Arctic. Of these lines, line #2 yields the smallest (best) repeatability of 0.43 mGal and best agreement between OIB and EGM2008 gravity with a standard deviation of 3.91 mGal. This is likely because the EGM2008 gravity model has relatively good surface gravity data coverage in the Canada Basin where Line # 2 is located. On the other hand, lines #1 and #3 lie in areas lacking good surface gravity data coverage. Nonetheless, gravity errors in the EGM2008 model over this Canada Basin area are appreciable. Note also that further results are listed for line #2 in Table 1 below—specifically that ARCS-2 predictions agree more closely with the OIB gravity (standard deviation of 2.57 mGal) than do EGM2008 predictions (standard deviation of 3.91 mGal).

[24] The remaining five OIB gravity lines presented here (see Figures 3, 4d–4h and Table 2 lines #4–#8) are not repeat flights unlike the first three OIB lines (#1–#3 in Table 1). Line #4 (see Figures 3 and 4d) of OIB gravity data was collected on the underflight of Envisat on 16 March 2011. Unlike line #2, the Envisat underflight of 5 April 2010 (Figure 4b), where outbound and return legs were flown at nearly the same elevations, outbound (segment 2) and return (segment 3) legs of line #4 were flown at distinctly different elevations (~450 and ~5200 m, respectively) which renders this OIB flight a non-repeat for the purposes of our gravity study. Only OIB gravity collected during the low-altitude (450 m) outbound segment 2 (see Figure 4d) are plotted. Inspection of Figure 4d, as well as the statistics listed for line #4 in Table 2, shows that the ARCS2 gravity model agrees more closely with OIB gravity observations than with the EGM2008 gravity model. A similar inspection of Figure 4b and the statistics listed for line #2 in Table 2 underscore that EGM2008 has significant apparent errors (4–6 mGal) even in the Canada Basin. Upon examination of lines #5 to # 8 in Table 2 along with Figures 4e–4h, large apparent gravity errors in the EGM2008 model are evident elsewhere in the Arctic Ocean. Assuming OIB gravity to be relatively error free, we see particularly large apparent EGM2008 errors along lines #7 and #8 in Table 2 (see Figures 4g and 4h), i.e., errors of order 20–40 mGal but of short (<125 km) wavelength. We speculate that the large OIB AirGrav gravity anomaly of approximately +50 mGal at 84.45N on line #7 (Figure 4g) may be associated with errors arising from the effects of aircraft maneuvering or turning (see data gap at 84.5°N) on processing and filtering the data adjacent to this gap [see Cochran et al., 2011]. Thus difference statistics on line #7 in Table 2 are shown to be large—with standard deviations of 11.23 mGal and 8.54 mGal for OIB gravity minus EGM2008 and ARCS2, respectively. While other OIB

Table 1. OIB Airborne Gravity Repeatability with OIB Gravity Filter Width = 100 s

Line #		Difference With EGM08		
		Repeatability RMS	Sdev	Mean Diff
1	OIB 17 March 2011 (Figure 4a)	0.62 mGal	5.65 mGal	2.56 mGal
2	OIB 5 April 2010 (Figure 4b)	0.43 mGal	3.91 mGal	-1.88 mGal
3 ^a	OIB 15 April 2011 (Figure 4c)	1.22 mGal	5.09 mGal	9.49 mGal

^aLine #3: Statistics computed for segment between 72.0°N and 80.0°N latitude. Flight elevation differed slightly between the repeat legs for Line #3.

Table 2. OIB Arctic Gravity Versus Gravity Model Predictions

Line #		Difference with EGM08		Difference with ARCS2	
		Sdev	Mean Diff	Sdev	Mean Diff
1	OIB 17 March 2011 (Figure 4a)	5.65 mGal	2.56 mGal	^a	^a
2	OIB 5 April 2010 (Figure 4b)	3.91 mGal	-1.88 mGal	2.57 mGal	-1.06 mGal
3	OIB 15 April 2011 (Figure 4c)	5.09 mGal	9.49 mGal	^b	^b
4	OIB 16 March 2011 (Figure 4d)	5.65 mGal	-3.60 mGal	3.44 mGal	-0.99 mGal
5	OIB 20 April 2010 (Figure 4e)	5.57 mGal	2.954 mGal	^a	^a
6	OIB 18 March 2011 s1 (Figure 4f)	6.75 mGal	5.96 mGal	^b	^b
7	OIB 18 March 2011 s2 (Figure 4g)	11.23 mGal	4.56 mGal	^c 8.54 mGal	4.41 mGal
8	OIB 28 March 2011 (Figure 4h)	8.66 mGal	8.56 mGal	9.98 mGal	-5.22 mGal

^aNo ARCS-2 gravity predictions for this line, all or most of which lies north of 86°N.

^bNo ARCS-2 gravity predictions for this line, which overlies Greenland and/or Ellesmere Island rather than the Arctic Ocean.

^cPossible large OIB air gravity errors due to P-3 maneuvers (see text and Figure 4g).

sea ice lines (e.g., #9 and #10) have been reflowed from year to year, line #7—a portion of the OIB 2011 “Zig-Zag West”—is not yet been repeated. Hopefully OIB will re-fly the line #7 portion of “Zig-Zag West” in 2013. The difference statistics, i.e., standard deviations, for both lines #7 and #8 are large (~8–10 mGal) possibly indicating intrinsic difficulty in recovering gravity from ICESat data in this area (no Envisat coverage here). Additional large apparent errors (of order 20 mGal or more) in EGM2008 gravity are also seen along other OIB lines, e.g., Line #1 and #3 (Figures 4a and 4c).

5. Arctic Geoids Errors: Effects on MDT Estimates

[25] The errors in EGM2008 gravity, which are described in section 4 above, are inferred along the OIB flight tracks and have associated geoid errors which can be accurately estimated only after making simplifying assumptions about off-track sources. For example, one can assume that source topography varies in only one dimension, e.g., along the direction of the flight track (see Appendix A). Accurate estimates of geoid error cannot be computed from a single, one-dimensional profile of gravity errors (e.g., Figures 4a–4h). Rather, one must begin with a two-dimensional characterization of gravity errors over the ocean and land surface and input those gravity errors to a Stokes integral transform. A highly accurate Arctic geoid requires accurate, densely spaced (at intervals of several km) near-surface gravity observations over the entire Arctic. The OIB gravity results in section 4 above indicate that errors of order 20 mGal owing to a lack of, or gaps in, precise gravity data are common across the Arctic Ocean. In sections 5.1 below, we show that associated errors in current Arctic geoid models of order several decimeters are also common and that these errors can corrupt estimates of MDT.

5.1. Geoid Versus Mean Sea Surface Topography: Detecting Geoid Errors

[26] Short-wavelength errors in existing geoid models of the Arctic present a greater obstacle to determining an accurate, detailed Arctic mean dynamic topography (MDT) [cf. *Farrell et al.*, 2012] than do geoid model errors over all other large ocean basins for corresponding determinations of the global ocean MDT [see, *Tapley et al.*, 2003]. *Farrell et al.* [2012] computed the Arctic MDT (h_{MDT} , for the ICESat epoch, 2003–2008) by differencing the new ICEn MSS (h_{MSS}), which was derived from ICESat as well as Envisat altimeter data, with an Arctic geoid (h_{G}), (i.e., $h_{\text{MDT}} = h_{\text{MSS}} - h_{\text{G}}$). They derived two different MDTs using two different geoids: (1) the EGM2008 geoid [*Pavlis et al.*, 2008] shown for the Arctic in Figure 5a and (2) the satellite-only GOCO02S geoid [*Goiginger et al.*, 2011]. An unfiltered version of the first MDT (Figure 5b) derived using the EGM2008 geoid reveals residual, predominantly short-wavelength uncertainties in both the EGM2008 geoid and the MSS field. Some MSS errors appear as ground track striations in this unfiltered MDT estimate (Figure 5b). However the geoid errors are generally larger magnitude than the MSS errors. These errors in the Arctic marine geoid range from several decimeters to as much as 1 m and arise where the EGM2008 model uses ArcGP as its primary input. ArcGP has large gaps in surface gravity data coverage in places, and, where necessary uses

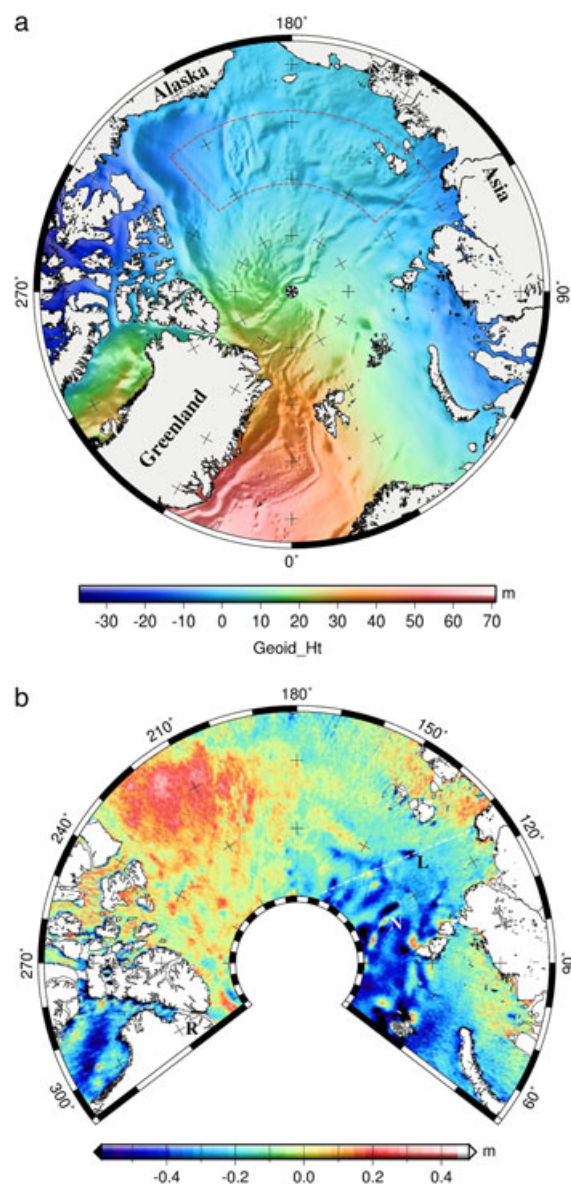


Figure 5. (a) Polar-stereographic map of the EGM2008 geoid [*Pavlis et al.*, 2008] for the Arctic. Geoid heights are with respect to Topex/Poseidon reference ellipsoid. Latitude-longitude box outlined with red dashes delineates the CBCLS region covered by the geoid error plots (Figures 7b and 7c) and discussed in section 5.2. (b) Plot of ICEn MSS [*Farrell et al.*, 2012] minus EGM2008 geoid for the Arctic Ocean which illustrates apparent dynamic topography such as the Beaufort Gyre (the broad, red high area in the Beaufort Sea north of Alaska) as well as geoid errors, some as large as 40–90 cm particularly in vicinity of Nansen-Gakkel Ridge (labeled N), the Robeson Channel (R) of the Nares Strait, and a dark blue (low) area in the northern Laptev Sea (labeled L). Note the white dashed line transecting area L is an ICESat ground track (pass 182; cf. Figure 6). *Farrell et al.* [2012] (see their Figures 3a and 3b) used low-pass filtering to suppress the effects of such geoid errors before computing mean dynamic topography.

early release ICESat data—particularly north of 81°N —in addition to satellite radar altimeter data to fill these gaps [*Andersen and Knudsen*, 2009]. Demonstrable errors in the

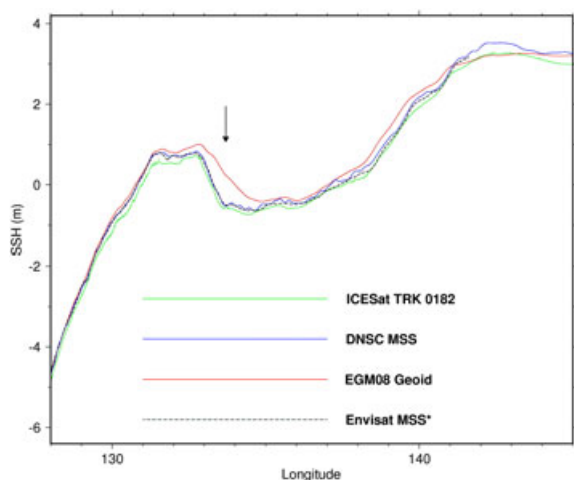


Figure 6. ICESat, Envisat, and DNSC08 MSS profiles along ICESat pass 0182 and transecting the MDT anomaly L in the northern Laptev Sea (Figure 5b), compared to the EGM2008 geoid. Arrow points to location of large (approximately +0.8 m) apparent geoid error.

Arctic component of EGM2008 geoid model manifest themselves as pseudo, short-wavelength structures in the MDT which tend to coincide with known, fine-scale bathymetric or gravimetric features. For example, these pseudo MDT structures include in Figure 5b: feature “N” over the Nansen-Gakkel ridge, feature “L” over the continental shelf edge in the northern Laptev, and feature “R” in the Robeson Channel of the Nares Strait. We suggest that these pseudo MDT structures result mostly from errors in the EGM2008 geoid (passed down from the ArcGP geoid). These geoid errors include a location in the Nansen-Gakkel, i.e., associated with feature “N” which is about 50 cm in magnitude, and over the shelf break in the northern Laptev Sea (feature “L”; see Figures 5b and 6) that is about +0.8 m. Over the southern Robeson Channel (feature “R” in the northern and central Nares Strait) both—or at least one of—geoid and MSS errors appear to be large—of order 50–90 cm. Comparison of EGM2008 and OIB gravity anomalies across the southern Robeson Channel between 78°N and 82°N (Figure 4f, above, as well as the profile in Figure 4c which lies just east of the Robeson Channel) indicate that EGM2008 gravity may be in error by -15 mGal on average (see Table 2, line #6) over a 500 km length and corroborate that the EGM2008 geoid may also be in error here by roughly -50 cm helping to give rise to the spurious, positive MDT anomaly “R” (Figure 5b).

[27] A more detailed study of the anomalous MDT low in the northern Laptev Sea (feature “L” in Figure 5b) is shown in Figure 6. Using a transect along ICESat pass 0182 through the center of the L anomaly, we compare the ICESat, Envisat, and DNSC08 MSS fields to EGM2008. A discrepancy of as much as 80 cm between the geoid model and three independent estimates of MSS height is evident between longitudes 133°E and 135°E which suggests that it is due to data gaps or errors in the ArcGP model, which was used in the EGM2008 geopotential model for the entire Arctic north of 60°N. Indeed these geoid errors may have resulted from using a subset of early-release ICESat altimetry [Andersen and Knudsen, 2009; Kenyon and Forsberg, 2008]

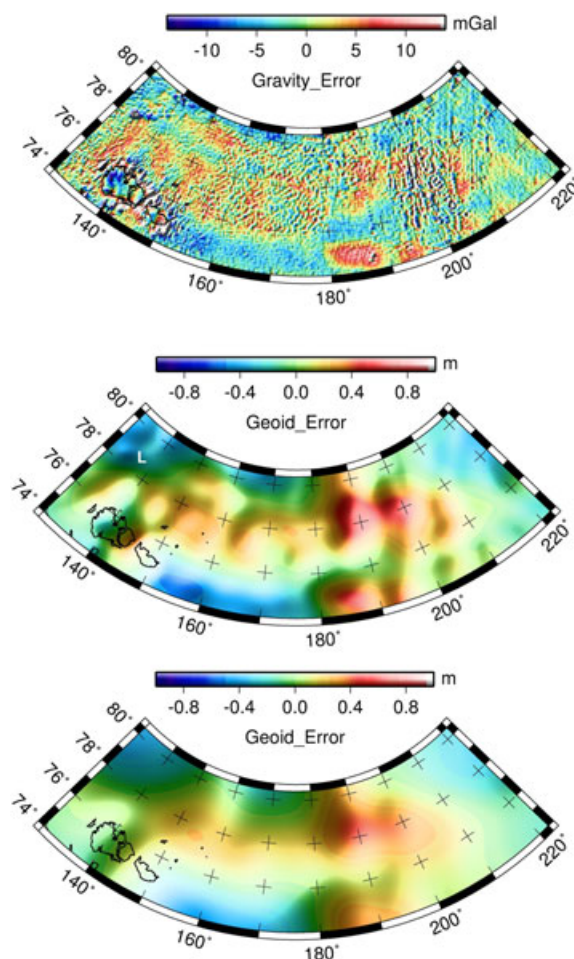


Figure 7. (a) ARCS-2 gravity minus EGM2008 gravity over the region of the Canada Basin-Chukchi-Laptev Sea (CBCL) region. Location delineated by dashed red line in Figure 5a. (b) Estimated geoid errors associated with EGM2008 or ARCS-2 model using Stokes transformation and 200 km Gaussian filtering. Geoid error at L (see text) is ~ 47 cm in magnitude. (c) Estimated geoid errors computed as in b above but smoothed instead with a 460 km Gaussian filter.

or tares in the surface gravity data sets employed in the ArcGP model.

5.2. Estimating Geoid Errors in the Canada Basin-Chukchi-Laptev Sea Region

[28] Here, errors in the Arctic geoid models, e.g., EGM2008, are estimated by first differencing the ARCS-2 gravity and EGM2008 gravity (see Figure 7a) over the region of the Canada Basin-Chukchi-Laptev Sea (CBCL) delineated with a dashed red line in Figure 5a. This CBCL region is chosen because evidence (e.g., the OIB gravity comparisons in section 4 such as Figures 4b and S3c) suggests EGM2008 gravity in the Canada Basin area is somewhat free of coverage gaps and large errors in gravity data. The Canada Basin is fairly well covered with surface gravity data and near surface airborne gravimetry [Childers *et al.*, 2001]. This CBCL region is also chosen to avoid land and coastal areas inasmuch as ARCS-2 is a marine gravity model. These gravity differences (Figure 7a) are taken as a measure of the

noise or errors in the two gravity fields. Assuming the noise or errors in each field, the ARCS-2 and EGM2008, are uncorrelated, independent, and random, we divide the gravity differences by the square root of 2 and then input them to the Stokes integral transform to estimate associated geoid errors. This Stokes transformation was accomplished in the spatial frequency domain using Fourier transformation tools in GMT [Wessel and Smith, 1998]. Oceanographic noise remaining in the ARCS-2 gravity field may cause geoid error estimates in this section to be slightly overstated. The estimated geoid errors are low-pass smoothed using (1) a modest 200 km Gaussian filtering (Figure 7b) and (2) a more intense 460 km Gaussian filtering (Figure 7c). In case (1), less filtering, the estimated geoid errors range from maximum of 58 cm to a minimum of -56 cm with a standard deviation of 22.9 cm; in case (2), more filtering, the estimated geoid errors range from max of 42 cm to a minimum of -39 cm with a standard deviation of 18.9 cm. To suppress geoid errors in estimating Mean Dynamic Topography (MDT), a Gaussian filtering, or kernel with a width of at least 250 m, is necessary (in fact Farrell et al. [2012] employ a 250 km Gaussian filter before computing Arctic MDT). The Gaussian kernel with width 100 km used by Kwok and Morison [2011] is therefore inadequate for suppressing Arctic geoid errors in EGM2008 and will retain large (of order 20 cm), spurious MDT “features” which are in fact geoid errors. Forsberg et al. [2007] also estimated an MDT using instead an MSS from ICESat and ERS-2 as well as an ArcGP geoid (virtually equivalent to the EGM2008 geoid) which they compared with Arctic Ocean circulation model estimates of MDT. However Forsberg et al.’s [2007] MDT estimates employed more smoothing than the 100 km Gaussian kernel used by Kwok and Morison [2011].

5.3. EGM2008 Versus GOCO2S Geoid in the Arctic

[29] The apparent errors in the Arctic geoid models discussed above, e.g., those which manifest themselves as MDT anomalies such as L, N and R in Figure 5b, are rather localized. Do such localized errors have a consequential, overall effect on a computed Arctic MDT [e.g., Farrell et al., 2012; Kwok and Morison, 2011] Can these geoid errors be effectively suppressed with low-pass filtering? And if so how much, or what sort of, low-pass filtering? To further address these questions we use a second, more conservative approach to geoid error estimation than that used in section 5.2 above. We now examine the difference between two different and nearly independent geoid models over the Arctic: (1) the GRACE/GOCE satellite-only model GOCO02S [Goinger et al., 2011] and (2) the EGM2008 [Pavlis et al., 2008] model. By differencing the space-based, fully gravimetric GOCO02S geoid with the EGM2008 geoid in the appropriate waveband we can constrain geoid errors in the EGM2008 model which are due in part to its inclusion of altimetry data. We thereby learn how these geoid models corrupt MDT determinations.

[30] Figure 8 shows the difference over the Arctic between these two geoid models (1) and (2), both computed to degree and order 250, after smoothing with a Gaussian filter of 250 km width. This 250 km filter is the same as that used by Farrell et al. [2012] to compute an MDT for the Arctic. This plot is an indicator of geoid errors at wavelengths of 250 km and longer. The RMS of the differences shown in

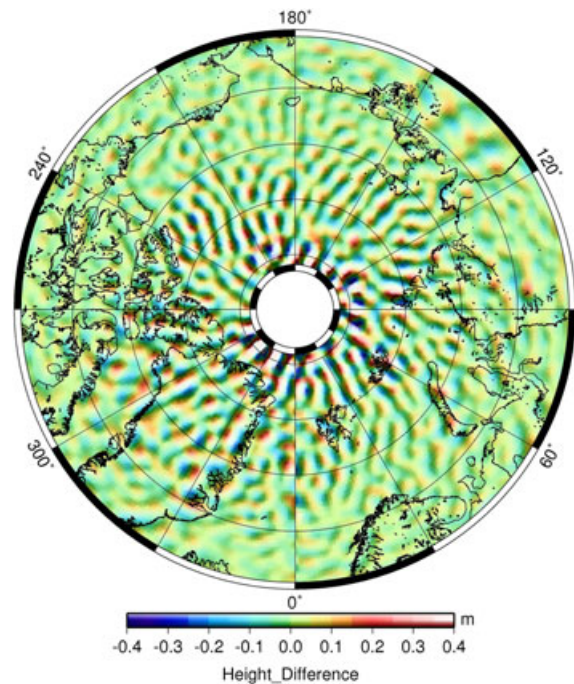


Figure 8. Geoid differences between GOCO02S and EGM2008 models over the Arctic with both models computed to degree and order 250 and smoothed with a low-pass Gaussian filter of width 250 km.

Table 3. RMS Differences Between GOCO02S and EGM2008 Arctic Geoid Models Computed to Degree and Order 250, After Smoothing With Various Gaussian Filters

Filter Width	Arctic (65°N to 85°N) Geoid Model RMS Differences
100 km	24.7 cm
150 km	19.1 cm
250 km	9.31 cm
360 km	5.93 cm

Figure 8 is 9.3 cm for the full latitude range 65°N–85.5°N. The RMS difference increase from south to north is likely due to gaps and errors in surface gravity observations tending to increase to the north in EGM2008. Data north of 85.5°N are not shown in Figure 8 because GOCE with its 96° inclination supplies essentially no gravity information for the GOCO02S model above 84°N. In consequence geoid differences north of this latitudinal limit are even larger. Geoid error results implied by Figure 8 show that apparent MDT features with wavelengths about 250 km (and longer) and amplitude of 10 cm or more [Farrell et al., 2012] are likely not artifacts of geoid error. The 250 km filtering of MDT is a good choice for suppressing short-wavelength errors in either the GOCO02S and EGM2008 geoids while retaining fair spatial resolution of MDT. Once again (cf. section 5.2), using a shorter Gaussian filter (of width 100–150 km) passes geoid errors of about 20–25 cm amplitude (Table 3). Therefore, apparent, fine-scale (of order 150 km wavelength) features in the Arctic MDT are more likely to be spurious and due to geoid errors rather than actual fine-scale ocean dynamics.

[31] Furthermore, PSD plots, Figures 9a–9d, spectrally decompose—and depict—the Arctic geoid noise versus

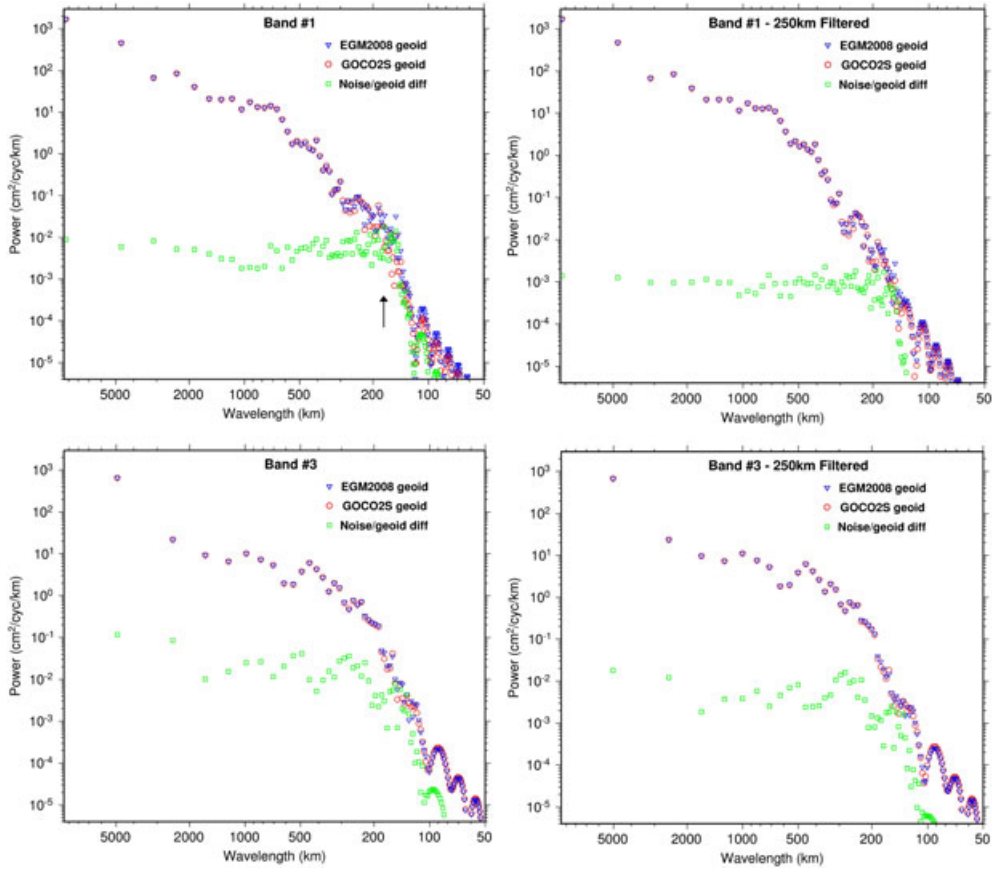


Figure 9. (a) Log-log graph of power spectral densities (PSDs) in meridional or longitude-dimension of (1) GOCO02S (in red) and (2) EGM2008 (blue) geoids computed to degree and order 250 along with PSDs (longitudinal) of differences (green) between (1) and (2) in the band #1 where latitudes ranges from 75.0°N to 79.5°N . The green difference PSDs indicate noise in geoid models. Vertical arrow at wavelength, 180 km, indicates where the noise PSD, in green, merges with the signal PSDs in red and blue. (b) Same as (a) except geoids have been smoothed with a 250-km Gaussian filter. (c) Same as Figure 9a except band of latitudes (#3) is more northerly—ranging from 81.0°N to 85.75°N . (d) Same as Figure 9c, i.e., northerly band of latitudes, #3, except geoids have been smoothed with a 250 km Gaussian filter.

signal obtained from the GOCO2S and EGM2008 geoid models in two latitude bands: the southern band (#1) of latitudes which ranges from 75.0°N to 79.5°N , and the northern band (#3) of latitudes which ranges from 81.0°N to 85.75°N . These results show that in the northern latitude band, #3, the noise/differences between geoid models (see green squares in Figure 9c) are larger than in the southern latitude band (see Figure 9a). The overall noise standard deviation associated with the northern band, #3, is 25.8 cm (before Gaussian smoothing) versus a noise standard deviation of 19.1 cm associated with the southern band, #1. After smoothing with 250 km width Gaussian filter, the corresponding noise standard deviation is 13.5 cm for the northern band, #3, and 7.2 cm for the southern band, #1 (see Figures 9b and 9d). Note the vertical arrow in Figure 9a at wavelength 180 km, which indicates where the noise PSD, in green, merges with the signal PSDs in green and blue. In other words the signal-to-noise ratio drops to 1.0 at about 180 km which can be seen to hold true for all four cases, Figures 9a–9d. This result of higher geoid noise in the northern latitudes, 81.0°N – 85.75°N , (i.e., band #3, see Figures 9c and 9d) indicates that one or both of the EGM2008 and GOCO geoid models have larger errors here than they do in the central/southern Arctic

(i.e., band #1). Even after a 250 km Gaussian smoothing, geoid errors in this northern band are large—with a standard deviation of about 13.5 cm for wavelengths >180 km. An oceanographic model [Zhang and Rothrock, 2003] indicates that corresponding MDT signal—with same 250 km Gaussian smoothing—in this same northern band #3 has a standard deviation of 14.1 cm almost the same as the 13.5 cm geoid noise. This shows how without aggressive smoothing geoid error or “noise” tends to overwhelm detailed MDT signal. So these results confirm that the state of current Arctic marine geoid models is such that we cannot confidently resolve MDT features with wavelengths much shorter than 250 km.

6. Conclusions

[32] The ARCS-2 gravity field presented in this paper is a high-resolution satellite-only Arctic marine field which provides more detail and higher spatial resolution than previous altimetric gravity models of the Arctic Ocean, e.g., the ARCS field [McAdoo et al., 2008]. ARCS-2 provides uniform, dense coverage of the Arctic Ocean from 67°N to 86°N including large areas of perennially ice-covered seas. ARCS-2 which is based purely on satellite data has been compared and

contrasted with surface gravity models such as EGM2008 of the Arctic derived mostly using independent, surface gravity observations. We have, thereby, outlined the type and location of surface—or near-surface—gravity observations that are needed to fill existing gaps in our knowledge of Arctic gravity. Recently collected, high-precision airborne gravity from NASA's Operation IceBridge (OIB Arctic 2010 and 2011 campaigns) has also been compared with EGM2008 gravity model predictions and thereby also used to help detect some significant errors in Arctic portions of EGM2008. Excellent repeatability, and hence precision, of OIB airborne gravity data has been demonstrated over the Arctic Ocean. Indeed flying a systematic network of OIB-like gravity lines may be the best way to produce the high-accuracy gravimetric geoid that is needed especially for Arctic Ocean circulation studies.

[33] Although the limiting factor in precisely determining absolute dynamic topography (MDT) from space for the large, global ocean basins may no longer be the precision and detail of the (satellite) geoid [see *Tapley et al.*, 2003]; we have also shown that geoid errors—as opposed to altimetric observations of sea surface topography—are the limiting factor for determining MDT over the Arctic Ocean basin. So, advancements in understanding permanent circulation of the Arctic Ocean will need to await an improved Arctic physical geodetic (e.g., gravity) data set. In addition ARCS-2 will be important for underpinning forthcoming Arctic altimetric gravity fields now being constructed using the new CryoSat-2 data

Appendix A

[34] Figures S1 and S2 show respectively the ICESat-only and Envisat only altimetric marine gravity field which are melded together (sections 3.1 and 3.3) to produce the final ARCS2 gravity field (Figure 1). Figures S3a and S3b show profiles of OIB airborne gravity collected on the April 19, 2010 DC-8 flight over the Chukchi Borderland and Canada Basin respectively (cf. Figure 2). Figure S3a compares gravity predictions of four different models with the OIB airborne gravity and the ARCS-2 seems to agree most closely with the OIB gravity. Figures S4 and S5 show year-to-year (2010 versus 2011) repeat OIB airborne gravity profiles. Note the excellent repeatability of better than 1 mGal despite the fact that different aircraft (DC-8 versus P-3B), flight speeds, and AIRGrav installation were involved.

[35] **Acknowledgments.** This paper is dedicated to our colleague and friend, Seymour Laxon, who died in a tragic accident on January 2, 2013. The authors acknowledge NASA's ICESat Science Project and the NSIDC for distribution of the ICESat data (see <http://nsidc.org/data/icesat/>), and ESA for the distribution of Envisat data. We also acknowledge the NASA Operation IceBridge (OIB) project team (<http://www.nasa.gov/icebridge/>) as well as NSIDC for the OIB AIRGrav data which are available at <http://nsidc.org/data/icebridge/index.html>. We also thank the OIB AIRGrav instrument team including J. Cochran, and R. Bell at Lamont Doherty Earth Observatory and colleagues at Sander Geophysics Ltd. for the high-quality OIB AIRGrav data. The views, opinions, and findings contained in this report are those of the authors and should not be construed as an official National Oceanic and Atmospheric Administration or U.S. Government position, policy, or decision.

References

Andersen, O. B., and P. Knudsen (2009), DNSCO8 mean sea surface and mean dynamic topography models, *J. Geophys. Res.*, *114*, C11001, doi:10.1029/2008JC005179.

Brozna, J. M., et al. (2003), New aerogeophysical study of the Eurasia Basin and Lomonosov Ridge: Implications for basin development, *Geology*, *31* September 2003, 825–828, doi:10.1130/G19528.1.

Carrere, L., and F. Lyard (2003), Modeling the barotropic response of the global ocean to atmospheric wind and pressure forcing—Comparisons with observations, *Geophys. Res. Lett.*, *30*(6), doi:10.1029/2002GL016473.

Childers, V. A., D. C. McAdoo, J. M. Brozna, and S. W. Laxon (2001), New gravity data in the Arctic Ocean: Comparison of airborne and ERS gravity, *J. Geophys. Res.*, *106*(B5), 8871–8886, doi:10.1029/2000JB900405.

Cochran, J. R., G. J. Kurras, M. H. Edwards, and B. J. Coakley (2003), The Gakkel Ridge: Bathymetry, gravity anomalies, and crustal accretion at extremely slow spreading rates, *J. Geophys. Res.*, *108*(B2), 2116, doi:10.1029/2002JB001830.

Cochran, J. R., M. H. Edwards, and B. J. Coakley (2006), Morphology and structure of the Lomonosov Ridge, Arctic Ocean, *Geochem. Geophys. Geosyst.*, *7*, Q05019, doi:10.1029/2005GC001114.

Cochran, J. R., and R. E. Bell (2010), IceBridge Sander AIRGrav L1B geolocated free air gravity anomalies, [March 2010–March 2011], Boulder, Colorado USA: NASA Distributed Active Archive Center at the National Snow and Ice Data Center, Digital media, <http://nsidc.org/data/iggrv1b.html>.

Cochran, J. R., S. Elieff, K. J. Tinto, and K. Charles (2011), IceBridge gravity instrument performance and data assessment, NASA Report, *in press*.

Farrell, S. L., D. C. McAdoo, S. W. Laxon, H. J. Zwally, D. Yi, A. L. Ridout, and K. A. Giles (2012), Mean dynamic topography of the Arctic Ocean, *Geophys. Res. Lett.*, *39*, L01601, doi:10.1029/2011GL050052.

Farrell, S. L., S. W. Laxon, D. C. McAdoo, D. Yi, and H. J. Zwally (2009), Five years of Arctic sea ice freeboard measurements from the Ice, Cloud and land Elevation Satellite, *J. Geophys. Res.*, *114*(C4), C04008, doi:10.1029/2008JC005074.

Ferguson, S., S. Elieff, R. Bell, and M. Studinger (2010), Measuring the gravity vector with an airborne gravimeter: Enhancing geoid measurements in remote areas (abstract) 2nd International Gravity Field Symposium, September 2010, Fairbanks, Alaska.

Forsberg, R., and H. Skourup (2005), Arctic Ocean gravity, geoid and sea ice freeboard from ICESat and GRACE, *Geophys. Res. Lett.*, *32*, L21502, doi:10.1029/2005GL023711.

Forsberg, R., et al. (2007), Combination of spaceborne, airborne and in-situ gravity measurements in support of Arctic Sea ice thickness mapping, *Danish National Space Center Technical Report, No. 7*, 137 pp., Copenhagen.

Giles, K. A., S. W. Laxon, D. J. Wingham, D. W. Wallis, W. B. Krabill, C. J. Leuschen, D. McAdoo, S. S. Manizade, and R. K. Raney (2007), Combined airborne laser and radar altimeter measurements over the Fram Strait in May 2002, *Remote Sens. Environ.*, *111*, 182–194, doi:10.1016/j.rse.2007.02.037.

Giles, K. A., S. W. Laxon, and A. L. Ridout (2008), Circumpolar thinning of Arctic sea ice following the 2007 record ice extent minimum, *Geophys. Res. Lett.*, *35*(22), doi:10.1029/2008GL035710.

Goinger, H., et al. (2011), The combined satellite-only global gravity field model GOCO02S, presented at the 2011 *General Assembly of the European Geosciences Union*, Vienna, Austria, April 4–8, 2011.

Grantz, A., S. D. May, P. T. Taylor, and L. Lawver (1990), Canada Basin, in *The Geology of North America*, vol. L, The Arctic Ocean Region, edited by A. Grantz, G. L. Johnson, and J. F. Sweeney, pp. 379–401, Geol. Soc. of Am., Boulder, Colorado.

Grantz, A., P. E. Hart, and V. A. Childers (2011), Geology and tectonic development of the Amerasia and Canada Basins, Arctic Ocean, in *Arctic Petroleum Geology*, Geol. Soc. Lond. Memoir 35, edited by A. M. Spencer, A. F. Embry, A. L. Gautier, A. V. Stoupakova, and A. K. Sørensen, pp. 771–799, The Geological Society of London, London, doi:10.1144/M35.50.

Haxby, W. F., G. D. Kerner, J. L. LaBrecque, and J. K. Weisell (1983), Digital images of 10 combined oceanic and continental data sets and their use in tectonic studies, *EOS 11 Trans. Am. Geophys. Un.*, *64*(52), 995–1004.

Heiskanen, W. A., and H. Moritz (1967), *Physical Geodesy*, 364 pp., W. H. Freeman and Company, San Francisco.

Jakobsson, M., R. Macnab, L. Mayer, R. Anderson, M. Edwards, J. Hatzky, H. W. Schenke, and P. Johnson (2008), An improved bathymetric portrayal of the Arctic Ocean: Implications for ocean modeling and geological, geophysical and oceanographic analyses, *Geophys. Res. Lett.*, *35*, L07602, doi:10.1029/2008GL033520.

Kenyon, S., and R. Forsberg (2008), New gravity field for the Arctic, *Eos Trans. AGU*, *89*(32), 289, doi:10.1029/2008EO320002.

Koenig, L., S. Martin, M. Studinger, and J. Sonntag (2010), Polar airborne observations fill gap in satellite data, *EOS Trans. AGU*, *91*(38), doi:10.1029/2010EO380002.

Kwok, R., H. J. Zwally, and D. Yi (2004), ICESat observations of Arctic sea ice: A first look, *Geophys. Res. Lett.*, *31*, L16401, doi:10.1029/2004GL020309.

Kwok, R., and J. Morison (2011), Dynamic topography of the ice-covered Arctic Ocean from ICESat, *Geophys. Res. Lett.*, *38*, L02501, doi:10.1029/2010GL046063.

Laxon, S. W., and D. C. McAdoo (1994), Arctic Ocean gravity field derived from ERS-1 satellite altimetry, *Science*, *265*, 621–624, doi:10.1126/science.265.5172.621.

- Laxon, S. (1994), Sea ice altimeter processing scheme at the EODC, *Int. J. Remote Sens.*, 15, 915–924.
- McAdoo, D. C., S. L. Farrell, S. W. Laxon, H. J. Zwally, D. Yi, and A. L. Ridout (2008), Arctic Ocean gravity field derived from ICESat and ERS-2 altimetry: Tectonic implications, *J. Geophys. Res.*, 113, B05408, doi:10.1029/2007JB005217.
- McAdoo, D. C., and K. M. Marks (1992), Gravity fields of the Southern Ocean from Geosat data, *J. Geophys. Res.*, 97(B3), 3247–3260; also corrigendum, v. 97, (B12), p 17709.
- Pail, R., et al. (2010), Combined satellite gravity field model GOCO01S derived from GOCE and GRACE, *Geophys. Res. Lett.*, 37, L20314, doi:10.1029/2010GL044906.
- Pavlis, N. K., S. Holmes, S. Kenyon, and J. K. Factor (2008), An Earth gravitational model to degree 2160, *Geophys. Res. Abstr.*, 10, EGU2008-A-01891.
- Peacock, N. R., and S. W. Laxon (2004), Sea surface height determination in the Arctic Ocean from ERS altimetry, *J. Geophys. Res.*, 109, C07001, doi:10.1029/2001JC001026.
- Rummel, R., W. Y. Yi, and C. Stummer (2011), GOCE gravitational gradiometry, *J. Geod.*, 85, 777–790, doi:10.1007/s00190-011-0500-0.
- Sandwell, D. T., and W. H. F. Smith (2009), Global marine gravity from retracked Geosat and ERS-1 altimetry: Ridge segmentation versus spreading rate, *J. Geophys. Res.*, 114, B01411, doi:10.1029/2008JB006008.
- Sandwell, D. T., and W. H. F. Smith (1997), Marine gravity anomaly from Geosat and ERS-1 satellite altimetry, *J. Geophys. Res.*, 102(B5), 10039–10054.
- Studinger, M., R. E. Bell, and N. Frearson (2008), Comparison of AIRGrav and GT-1A airborne gravimeters for research applications, *Geophysics*, 73, 151–161.
- Tapley, B. D., S. Bettadpur, M. Watkins, and C. Reigber (2004), The gravity recovery and climate experiment: Mission overview and early results, *Geophys. Res. Lett.*, 31, L09607, doi:10.1029/2004GL019920.
- Tapley, B. D., D. P. Chambers, S. Bettadpur, and J. C. Ries (2003), Large scale ocean circulation from the GRACE GGM01 Geoid, *Geophys. Res. Lett.*, 30(22), 2163, doi:10.1029/2003GL018622.
- Taylor, P. T., L. C. Kovacs, P. R. Vogt, and G. L. Johnson (1981), Detailed aeromagnetic investigations of the Arctic Basin: 2, *J. Geophys. Res.*, 86(B7), 6323–6330, doi:10.1029/JB086iB07p06323.
- Vening Meinesz, F. A. (1928), A formula expressing the deflection of the vertical of the plumb-line in the gravity anomalies and formulae for the gravity field and the gravity potential outside the geoid, *Proc. Koninkl. Ned. Akad. Wetenschap.*, 36(3), 315–331.
- Wessel, P., and W. H. F. Smith (1998), New, improved version of generic mapping tools released, *EOS Trans. AGU*, 79, 579, doi:10.1029/98EO00426.
- Wingham, D. J., et al. (2006), CryoSat: A mission to determine the fluctuations in Earth's land and marine ice fields, *Adv. Space Res.*, 37(4), 841–871, doi:10.1016/j.asr.2005.07.027.
- Wunsch, C., and E. M. Gaposchkin (1980), On using satellite altimetry to determine the general circulation of the ocean with application to geoid improvement, *Rev. Geophys.*, 18, 725–745.
- Yi, D., H. J. Zwally, and J. W. Robbins (2011), ICESat observations of seasonal and interannual variations of sea-ice freeboard and estimated thickness in the Weddell Sea, Antarctica (2003–2009), *Ann. Glaciol.*, 52(57), 43–51.
- Zhang, J. L., and D. A. Rothrock (2003), Modeling global sea ice with a thickness and enthalpy distribution model in generalized curvilinear coordinates, *Mon. Weather Rev.*, 131, 845–861.
- Zwally, H. J., D. Yi, R. Kwok, and Y. Zhao (2008), ICESat measurements of sea ice freeboard and estimates of sea ice thickness in the Weddell Sea, *J. Geophys. Res.*, 113, C02S15, doi:10.1029/2007JC004284.
- Zwally, H. J., et al. (2002), ICESat's laser measurements of polar ice, atmosphere, ocean and land, *J. Geodyn.*, 34(3-4), 405–445, doi:10.1016/S0264-3707(02)00042-X.